

## Effect of Morphology on the Thermodynamic function of A-TiO<sub>2</sub> Nano-Materials

Jing Luo<sup>1,2</sup>, Xiaohua Yu<sup>3</sup>, Shiyong Li<sup>1,2\*</sup>, Ruijia Diao<sup>3</sup>

<sup>1</sup> Fire Research Institute, Southwest Forestry University, Kunming 650024, China

<sup>2</sup> College of Civil Engineering, Southwest Forestry University, Kunming, 650024, China;

<sup>3</sup> Faculty of Material Science and Engineering, Kunming University of Science and Technology, Kunming 650093, China.

\*E-mail: [lincoln558@163.com](mailto:lincoln558@163.com)

Received: 9 April 2019 / Accepted: 14 June 2019 / Published: 30 June 2019

The thermodynamic functions of A-TiO<sub>2</sub> nano-materials with different shapes (nanowires, nanotubes, nanoflakes and nanoparticles) were investigated by Faraday's law and open-circuit potentiometry. The results showed that the A-TiO<sub>2</sub> nanoparticles have the highest chemical activity (nanoparticles > nanoflakes > nanotubes > nanowires) at the same size, and the corresponding free energies and enthalpy are  $\Delta G = -895.59 \text{ kJ} \cdot \text{mol}^{-1}$ ,  $\Delta S = 76.09 \text{ J} \cdot \text{K}^{-1} \cdot \text{mol}^{-1}$ ,  $\Delta H = 847.21 \text{ kJ} \cdot \text{mol}^{-1}$ ; However, the stability of A-TiO<sub>2</sub> nanowires is the best (nanowires > nanotubes > nanoflakes > nanoparticles), and the ionic diffusion coefficient is lower than other structures (nanowires < nanotubes < nanoflakes < nanoparticles). There are more surface-active spots in nanometer-sized A-TiO<sub>2</sub>, which makes it more likely to lose electrons in the equilibrium state. This work intends to provide a reference for the design and analysis of various nanostructured materials.

**Keywords:** Nanostructure; A-TiO<sub>2</sub>; Thermodynamic property; Diffusion coefficient; Form effect

### 1. INTRODUCTION

TiO<sub>2</sub> is widely used in the fields of material anticorrosion, lithium ion battery development, catalysis, and sewage treatment due to its environmentally friendly, low-cost, and stable structure [1-4]. Anatase TiO<sub>2</sub> (A-TiO<sub>2</sub>) is the most popular activity material in the three crystalline forms of TiO<sub>2</sub> (anatase, rutile and plate titanium) [5]. However, it is a pity that A-TiO<sub>2</sub> is a wide band-gap semiconductor, and its chemical activity and stability are difficult to coordinate, this brings great challenge to the theoretical design of A-TiO<sub>2</sub> materials [6, 7].

Thermodynamic function is the essence of the control and design of nanomaterials, it is of great value to explain the inherent law of nanomaterials [8]. In fact, most of the current studies have focused

on hydrothermal [9], anodic oxidation [10], atomic layer deposition [11] and other fields of synthesis and doping modification [12]. It has been proven that the nanometer size effect has a great influence on the properties of the materials, and that the properties of the same materials with different nanostructures are not the same. It is difficult to compare and explain the mechanism of interaction between different morphologies. For example, it was reported that A-TiO<sub>2</sub> nanoparticles have high activity [13]. However, it was also reported that A-TiO<sub>2</sub> nanotubes have high activity [14-16]. Earlier studies from our group have shown that the thermodynamic function of nanomaterials can be evaluated by Faraday's law and the open-circuit potential method [17-19]. Therefore, to explain the difference of A-TiO<sub>2</sub> nanomaterials with different morphologies (nanowires, nanotubes, nanoflakes and nanoparticles) a thermodynamic function has been used in the present study. The method used herein can be used as a reference for characterizing the properties of the same materials with different nanostructures in future studies.

In this work, based on the X-ray diffraction (XRD), X-ray photoelectron spectroscopy (XPS), scanning electron microscopy (SEM), open circuit potential, and electrochemical impedance spectroscopy (EIS), the microstructure, phase composition, electrochemical activity and stability of the A-TiO<sub>2</sub> nanocrystalline was investigated.

## 2. MATERIALS AND METHODS

In order to make properties comparable, A-TiO<sub>2</sub> nanowires (between 120 and 160nm in diameter, NWs), A-TiO<sub>2</sub> nanotubes (between 100 and 160nm in pipe diameters, NTs), A-TiO<sub>2</sub> nanowires (between 50 and 80nm in thickness, NFs), A-TiO<sub>2</sub> nanoparticles (between 100 and 180nm in diameters, NPs), A-TiO<sub>2</sub> bulk (purity ≥ 99.0%), and Ti(SO<sub>4</sub>)<sub>2</sub> (purity ≥ 96.0%) were all purchased from Aladdin (Shanghai, China).

In this work, the activity of A-TiO<sub>2</sub> is measured by electrochemical methods. The electrode preparation methods are as follows: 1 ) A glassy carbon (GC) electrode was polished by Al<sub>2</sub>O<sub>3</sub> powder with different particle sizes, then the GC electrode was cleaned by an ultrasonic cleaning process using acetone, anhydrous ethanol, nitric acid and deionized water for 5 min respectively. 2 ) the A-TiO<sub>2</sub> nanomaterials and A-TiO<sub>2</sub> bulk of the same amount (5mg) were dissolved in the absolute ethanol of 0.1mL, respectively, and dispersed by ultrasound for 1h. 3 ) the 10 μL dispersed A-TiO<sub>2</sub>-ethanol solution was transferred and dropped onto the GC electrode, when the solution was dried, then the 5% nafion solution was coated over the GC electrode and dried in the air.

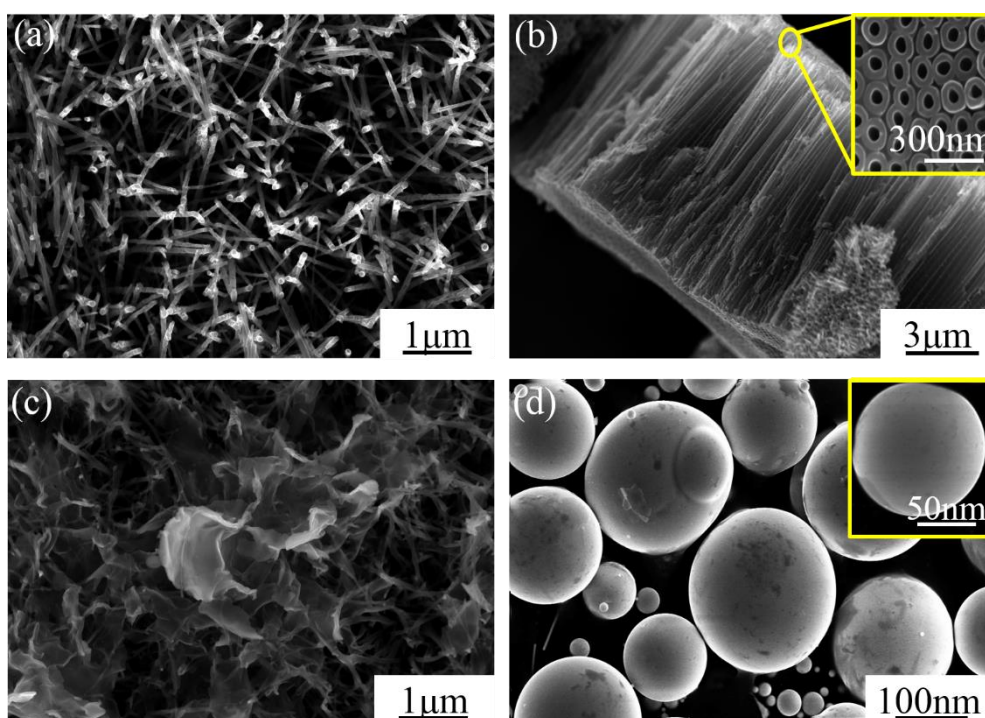
Open circuit potential tests were carried out using a two electrode system in which the A-TiO<sub>2</sub> bulk and A-TiO<sub>2</sub> nanomaterials with different structures acted as anode and cathode, respectively. The open circuit potential curve was measured at 288.15 K, 298.15 K, 308.15 K, 318.15 K, 328.15 K for 30s, then the electrode treatment steps were repeated and 5 parallel experiments were carried out on each sample; finally, the mean value of the 5 experiments was taken. The electrolytes of the open circuit and EIS test were a solution of 0.4mmol L<sup>-1</sup> Ti(SO<sub>4</sub>)<sub>2</sub> + 1mmol L<sup>-1</sup> H<sub>2</sub>SO<sub>4</sub> and a solution of 0.5mol L<sup>-1</sup> LiNO<sub>3</sub>, respectively.

The microstructures of the samples were observed using an SEM (EVO MA 10/LS 10; Carl Zeiss, Jena, Germany). The phases of nanomaterials were analyzed by power X-ray diffraction (PW 1830/00; Philips, Holland) using Cu K $\alpha$  radiation (0.15406 nm). The valence state of the elements were obtained from XPS measurements (PHI-5000 Versa probe IIIU Ivac-Phi; Japan) using aluminum as the ray source. Raman scattering was collected at room temperature using a DXR Raman spectrometer with a 5 nm laser source from an Ar<sup>+</sup> laser. Electrochemical measurements were conducted using a CHI760e electrochemical analyzer (CH Instruments, Shanghai, China).

### 3. RESULTS AND DISCUSSION

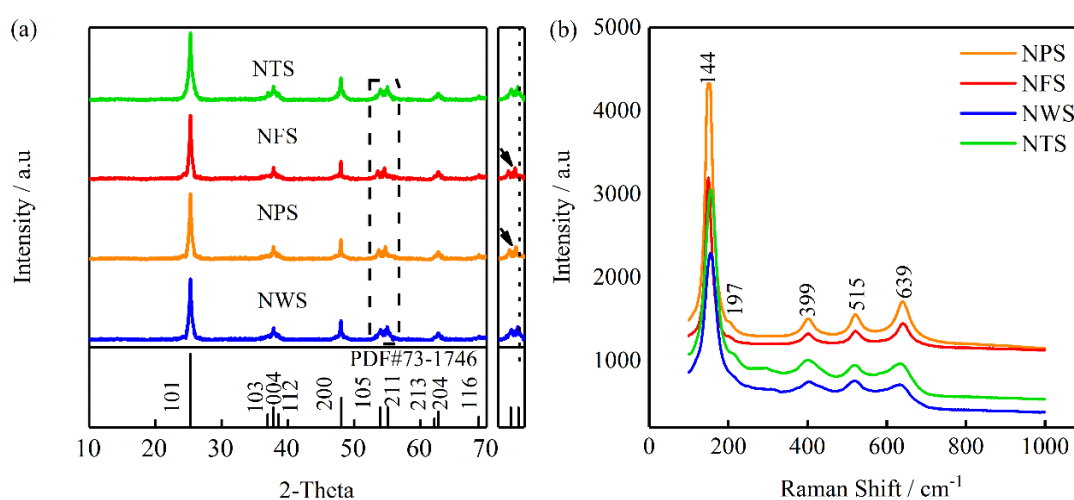
#### 3.1 Microscopic morphology and phase structure analysis

Fig. 1 shows the microstructure of the A-TiO<sub>2</sub> nanomaterials with different structures. As shown in Fig. 1(a), A-TiO<sub>2</sub> has obvious linear structure with a radius of about 60-80 nm. The length of nanowires reaches the micron level and the diameter of each nanowires is almost uniform along the length of the nanowires. The A-TiO<sub>2</sub> nanotube array has a regular and uniform structure with a tube diameter of about 100-160nm, in which the wall thickness of the tube is about 50-80nm (Fig. 1(b)). Fig. 1(c) shows the A-TiO<sub>2</sub> has a distinct sheet structure with a relatively uniform size, an average thickness of about 50 to 80 nm. A granular nanostructure of A-TiO<sub>2</sub> is showed in Fig. 1(d), with a uniform size and an average radius of about 50-80 nm. Generally speaking, all samples with linear, tubular, flake and granular structures have similar nanoscale sizes and the condition of forming the nano-electrode is satisfied.



**Figure 1.** Microstructure of pure A-TiO<sub>2</sub> (a)NWs, (b)NTs, (c)NFs, (d)NPs

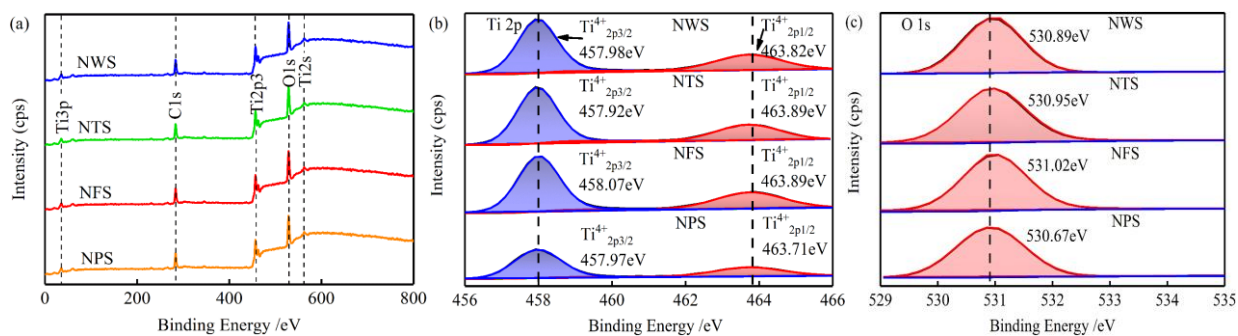
The diffraction peak of A-TiO<sub>2</sub> with a different morphology is similar to the standard A-TiO<sub>2</sub> (PDF#73-1746), and all the A-TiO<sub>2</sub> showed anatase structure (Fig. 2(a)). The (105) and (121) X-ray diffraction peaks of A-TiO<sub>2</sub> nanoparticles and A-TiO<sub>2</sub> nanoflakes shifted to different degrees respectively. This is due to the lattice distortion of nanoparticles and nanoflakes. It is important to note that no other crystalline phases were observed in X-ray diffraction peaks, such as rutile. Fig. 2(b) shows the Raman spectra of the A-TiO<sub>2</sub> nanomaterials. There are six characteristic peaks of anatase titanium dioxide: 144 cm<sup>-1</sup>, 197 cm<sup>-1</sup>, 399 cm<sup>-1</sup>, 515 cm<sup>-1</sup>, 519 cm<sup>-1</sup> (coincident with 515cm<sup>-1</sup>) and 639cm<sup>-1</sup> [20], thus it is proven that all four structures of A-TiO<sub>2</sub> are typical anatase phase structures. The blue shift of the strongest peak of 114 cm<sup>-1</sup> of the nanowires and nanotubes is attributed to the crystal size and non-stoichiometric structure [21].



**Figure 2.** (a) XRD patterns of pure A-TiO<sub>2</sub> with different structures, (b) Raman spectra of pure A-TiO<sub>2</sub> with different structures

### 3.2 XPS spectra of the nanomaterials

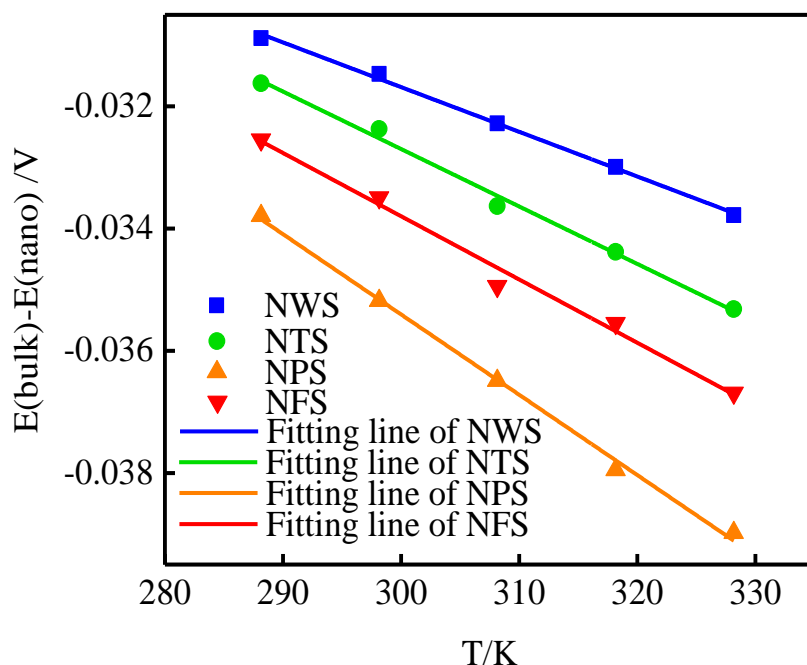
To further study the microstructure of nanomaterials, the XPS spectra of A-TiO<sub>2</sub> is shown in Fig. 3. All spectra were calibrated using the adventitious C 1s peak with a fixed potential of 284.6 eV. An external standard method was used to calibrate the X-ray photoelectron spectrometers. By comparing the broad spectrum of the four structures (Fig. 3(a)), it can be seen that their elemental composition was the same and the elements with highest abundance were C, Ti, and O. Fig. 3(b) shows that the narrow spectra of Ti2p of the four structures of A-TiO<sub>2</sub> resulted from two overlapping peaks. The binding energies (BE) of 457.98, 458.92, 458.07 and 457.97eV represent Ti<sub>2p3/2</sub><sup>4+</sup>, whereas BE values of 463.82, 463.89 and 463.71eV represent Ti<sub>2p1/2</sub><sup>4+</sup>. These results indicate that all the structures of the A-TiO<sub>2</sub> contained Ti<sup>4+</sup>. Fig. 3(c) indicates that the narrow spectra of O1s of the four structures of A-TiO<sub>2</sub> resulted from one peak. The BEs of 530.89, 530.95, 531.02, 530.67eV represent O<sup>2-</sup>. These results indicate that oxygen was present in the different structures O<sup>2-</sup>. According to the Ti 2p and O 1s spectra of the samples, the four structures of A-TiO<sub>2</sub> were determined to contain TiO<sub>2</sub>.



**Figure 3.** XPS spectra of pure A-TiO<sub>2</sub>, (a) survey spectrum, (b) Ti 2p, (c) O 1s

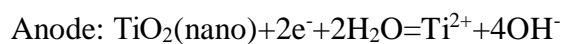
### 3.3 OCP measurements

Fig. 4 shows the electrode potential difference as a function for two electrodes at different temperature. The relationship between potential difference and temperature is linearly fitted, and the fit line is also displayed in Fig. 4.



**Figure 4.** Electrode potential difference as a function for two electrodes immersed in the 0.4mmol L<sup>-1</sup> Ti(SO<sub>4</sub>)<sub>2</sub> + 1mmol L<sup>-1</sup> H<sub>2</sub>SO<sub>4</sub> at different temperature

The potential difference of the primary battery composed of the bulk A-TiO<sub>2</sub> electrode and the four kinds of nano-A-TiO<sub>2</sub> electrodes increases linearly with the increase of temperature. The electrode reactions are as follows:



Compared with bulk materials, nanomaterials have higher energy and are more likely to react in the equilibrium state. Therefore, in the primary battery composed of bulk A-TiO<sub>2</sub> electrode and nano-A-TiO<sub>2</sub> electrode, nano-A-TiO<sub>2</sub> more easily attracts electrons and facilitates a reduction reaction, so the nanoelectrode has a higher potential and becomes the anode of the primary battery. This result is similar to the study of Xue et al [22-23], their research suggests that at the nanometer size, the smaller the size, the more unstable the silver oxide is. In this research, each of the nano A-TiO<sub>2</sub> systems are similar in size, thus the stability of nano A-TiO<sub>2</sub> with different morphological structures is tested with respect to how they differ from each other; their differing electrochemical properties may be due to the difference in specific surface area and surface defect concentration.

The fitting results are in accordance with the formula  $E=A+BT$  [24]. The temperature coefficient  $(\partial E/\partial T)_p$  of the potential difference between the bulk electrode and the nano-electrode with different structures can be obtained by the derivative of the formula. The fitting results and the temperature coefficients are listed in Table 1.

**Table 1.** The parameter of fitting line ( $R^2$  is the square of the linear correlation coefficient)

sample	A	B/10 <sup>-5</sup> (V/K)	R <sup>2</sup>
NWs	-0.031	-7.320	0.998
NTs	-0.032	-9.410	0.994
NFs	-0.033	-13.100	0.989
NPs	-0.034	-10.40	0.997

### 3.4 Thermodynamic function Properties of nano-A-TiO<sub>2</sub>

Fig. 5 shows the Gibbs free energy, entropy and enthalpy calculated by Faraday's law. The thermodynamic equations are as follows[24-26]:

$$\Delta S_m^\ominus = S_{m,TiO_2(bulk)}^\ominus - S_{m,TiO_2(nano)}^\ominus = zF \left( \frac{\partial E^\ominus}{\partial T} \right)_p \quad (1)$$

$$(\Delta_r G)_{T,P} = W_{f,max} = -zE^\ominus F = \Delta_f G_{m(bulk)}^\ominus - \Delta_f G_{m(nano)}^\ominus \quad (2)$$

$$(\Delta_r G)_{T,P} = W_{f,max} = -zE^\ominus F = \Delta H - T\Delta S^\ominus \quad (3)$$

It is worth noting that a striking differences existed between the thermodynamic functions of A-TiO<sub>2</sub> with different nano-structures. The Gibbs free energy of all nano-A-TiO<sub>2</sub> is higher than that of bulk A-TiO<sub>2</sub> (-888.80kJ · mol<sup>-1</sup>[27]) (Fig. 5(a)), The Gibbs free energy of nanoparticles is the highest (-894.87kJ · mol<sup>-1</sup>), which is slightly higher than the other A-TiO<sub>2</sub> nanostructures (nanoparticles >

nanoflakes > nanotubes > nanowires), the difference between the highest and lowest Gibbs free energy is about  $0.72\text{kJ}\cdot\text{mol}^{-1}$ . The results indicate that when the size of nanostructures is closed, the A-TiO<sub>2</sub> nanoparticles have highest activity among the different A-TiO<sub>2</sub> nanostructures. Fig. 5(b) shows the entropy of nano-A-TiO<sub>2</sub> with different structures. The entropy of all nano-A-TiO<sub>2</sub> is higher than that of bulk A-TiO<sub>2</sub> ( $50.62\text{J}\cdot\text{K}^{-1}\cdot\text{mol}^{-1}$ ) and the entropy of nanoparticles is the highest ( $76.09\text{J}\cdot\text{K}^{-1}\cdot\text{mol}^{-1}$ ) in the different nanostructures. Compared with the A-TiO<sub>2</sub> nanowires with the lowest entropy, the entropy is increased by  $11.34\text{J}\cdot\text{K}^{-1}\cdot\text{mol}^{-1}$ . Moreover, Fig. 5(c) shows the entropy of nano-A-TiO<sub>2</sub> with different structures. The enthalpy of all nano-A-TiO<sub>2</sub> is higher than that of bulk A-TiO<sub>2</sub> ( $-944.00\text{kJ}\cdot\text{mol}^{-1}$ ) and the enthalpy of nanoparticles is the highest ( $-947.21\text{kJ}\cdot\text{mol}^{-1}$ ) in the different nanostructures. Due to nanometer size, the proportion of surface activated atoms of the nanomaterial notably increased, which lead to the significant increase of entropy; the notable increase of the proportion of activated atoms resulted in a metastable state of the nano system, which was shown as the enthalpy increased evidently. The addition of Gibbs free energy shows that the nanometer size material can react more easily. Furthermore, the four structures of A-TiO<sub>2</sub> have a different content of defects; the nanoparticles had the largest activated specific surface area with a large number of defects as compared with the other structures in closed nanometer size. This results in the A-TiO<sub>2</sub> nanoparticles having a larger Gibbs free energy and correspondingly it can react more easily [2].

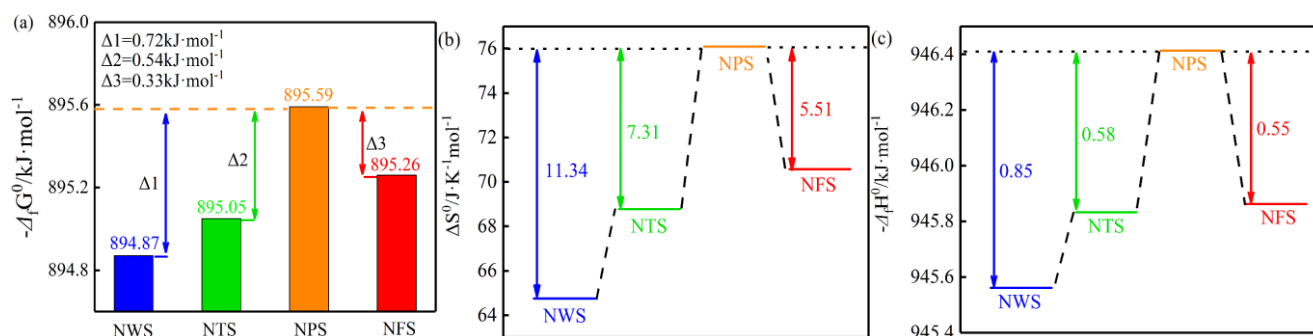


**Figure 5.** The value of Gibbs free energy, entropy and enthalpy of nano-A-TiO<sub>2</sub> calculated by Eq.(1-3)

### 3.5 AC impedance analysis

The EIS data of the nano-A-TiO<sub>2</sub> with different structures immersed in the 0.5M LiNO<sub>3</sub> solution at 25 °C is shown in Fig. 6(a). As can be seen, the Nyquist plots show that all A-TiO<sub>2</sub> samples exhibited an incomplete and capacitive-like semi-circle (The equivalent circuit is also attached to Fig. 6 (a)), in which the equivalent original CPE and  $R_{ct}$  was used instead of the double layer capacitance and charge transfer resistance, respectively.  $R_s$  represents the solution resistance. As shown in Table 2, the fitted  $R_{ct}$  value of nano TiO<sub>2</sub> is closed to the Li et al [28, 31]. As compared with some of the reported TiO<sub>2</sub> with various nano-scale structures, the value of  $R_{ct}$  is similar, and the value of  $\sigma$  is lower, because the size of the nano-structures is lower and the large Gibbs free energy in this work; as shown by the comparison made in Table 3, the fitted  $R_{ct}$  value of A-TiO<sub>2</sub> nanoparticles is lower than other structures. Due to the largest Gibbs free energy of nanoparticles, which corresponds to less stability, and consequently a lower

resistance. The  $W$  was Warburg impedance arising from the semi-infinite diffusion of  $\text{Li}^+$  in the electrode, which is relative to  $Z_{re}-\sigma$  obtained from the slope of the fitting line in Fig. 6 (b).

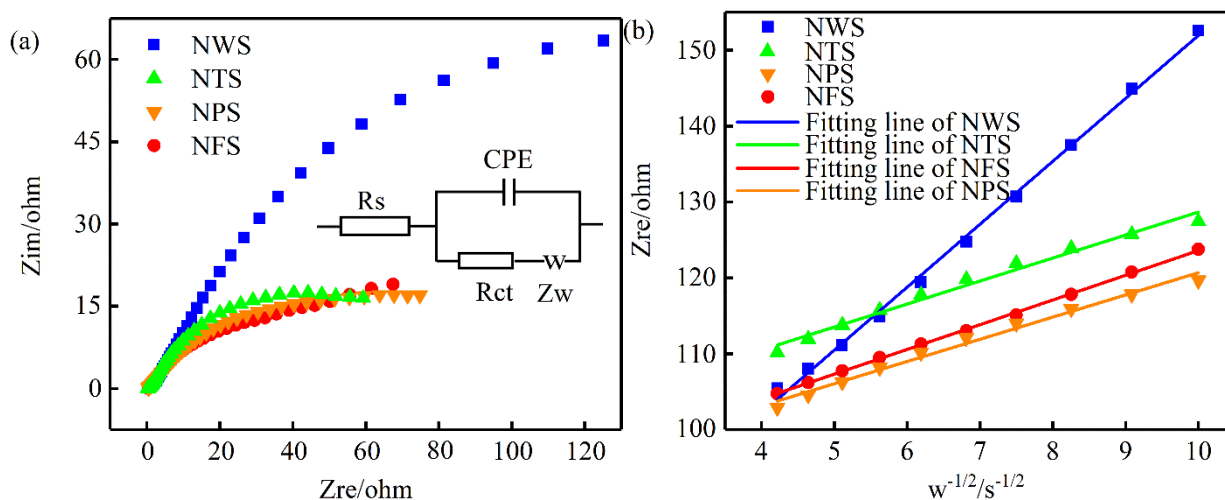


**Figure 6.** (a) Nyquist plots of the A-TiO<sub>2</sub> electrodes immersed in the 0.5M LiNO<sub>3</sub> solution at 25 °C, the inset: the corresponding equivalent circuit, (b) the real part of the impedance versus  $\omega^{-1}$  of A-TiO<sub>2</sub> electrodes

**Table 2.** The element parameters obtained by fitting EIS data

sample	$R_s$ ( $\Omega \text{ cm}^2$ )	$R_{ct}$ ( $\Omega \text{ cm}^2$ )	$\sigma$ ( $\Omega \text{ cm}^2 \text{ s}^{-0.5}$ )
NWs	13.160	72.030	8.274
NTs	13.020	64.670	3.028
NFs	12.980	60.390	3.231
NPs	13.050	58.860	2.921

**Table 3.** The comparison of the electrochemical properties of the TiO<sub>2</sub> as anode materials for lithium-ion batteries.

Refs	Sample	Morphology	$R_{ct}$ ( $\Omega/\text{cm}^2$ )	$\sigma$ ( $\Omega\text{cm}^2\text{s}^{-0.5}$ )
[28]	TiO <sub>2</sub>	NPs	57	8.457
[29]	TiO <sub>2</sub>	NPs	64±2.5	--
[30]	TiO <sub>2</sub>	NTs	77.150	--
This work	TiO <sub>2</sub>	NPs	58.860	2.921
	TiO <sub>2</sub>	NTs	72.030	3.028

The radius of the semi-circle relative to the A-TiO<sub>2</sub> nanoflakes was obviously smaller than the other nanostructures, followed by the A-TiO<sub>2</sub> nanoparticles, indicating that the A-TiO<sub>2</sub> nanoflakes and nanoparticles have low resistance and a high electron transfer rate. In addition, the radius of the

semicircle relative to the A-TiO<sub>2</sub> nanowires was largest, indicating that the blocking effect on the charge movement of A-TiO<sub>2</sub> nanowires is relatively large. In addition, it can be seen that the fitting line corresponding to the A-TiO<sub>2</sub> nanoparticles has the smallest slope and the smallest Warburg factor. On the contrary, that of the A-TiO<sub>2</sub> nanowires has the maximal slope of its fitting line ( $\sigma=8.274\Omega\text{ cm}^2\text{ s}^{-0.5}$ ).

Additionally, Li<sup>+</sup> diffusion coefficient ( $D$ ) can also be calculated according to the following Eq. 1[32]:

$$D = R^2 T^2 / (2A^2 n^4 F^4 C^2 \sigma^2)$$

Where  $R$  is the ideal gas constant,  $T$  is the absolute temperature,  $A$  is the electrode area,  $n$  is the number of electrons transferred in the reaction of the redox couple,  $F$  is Faraday constant, and  $C$  is the concentration of Li<sup>+</sup> in the solution. Therefore, the ion diffusion coefficient is inversely proportional to the Warburg factor, and the diffusion coefficient of A-TiO<sub>2</sub> nanoparticles is higher than that of other structures (nanoparticles > nanotubes > nanoflakes > nanowires); this is beneficial to the diffusion of ions in the electrode. The data indicates that the A-TiO<sub>2</sub> nanoparticles electrodes exhibited faster electrochemical kinetics and a smaller polarization.

#### 4. CONCLUSIONS

1) Due to the higher activity of nano-A-TiO<sub>2</sub> electrodes, the electrode potential of the primary battery composed of nano-A-TiO<sub>2</sub> electrode and bulk A-TiO<sub>2</sub> electrode is different, and the potential difference increases linearly with the increase of the temperature.

2) According to the temperature coefficient, the Gibbs free energy, entropy and enthalpy of nano-A-TiO<sub>2</sub> with different structures were calculated. At the same size, A-TiO<sub>2</sub> nanoparticles exhibit the best thermodynamic properties; the Gibbs Free Energy increased from -888.8 kJ·mol<sup>-1</sup> of bulk A-TiO<sub>2</sub> to -894.87 kJ·mol<sup>-1</sup>, the entropy increased from 50.62 J·K<sup>-1</sup>mol<sup>-1</sup> of bulk A-TiO<sub>2</sub> to 76.09 J·K<sup>-1</sup>mol<sup>-1</sup>, and the enthalpy increased from -944 kJ·mol<sup>-1</sup> of bulk A-TiO<sub>2</sub> to -947.213 kJ·mol<sup>-1</sup>.

3) The A-TiO<sub>2</sub> nanoparticles showed lower resistance and a higher diffusion coefficient of Li<sup>+</sup> ions. This is due to the outstanding thermodynamic properties of A-TiO<sub>2</sub> nanoparticles and the larger number of reaction sites on the surface, resulting in a significant improvement in electrochemical performance.

#### ACKNOWLEDGEMENTS

This work was supported financially by the Education Department Scientific Research Project of Yunnan Provincial (No. 2019J0195).

#### References

1. T. Luttrell, S. Halpegamage, J. Tao, *Sci. Rep.UK*, 4 (2014) 4043.
2. Z. P. Xie, Z. W. Wang, Y. X. Hua, *Mater. Res. Express*, 6 (2019) 046418.
3. Q. Guo, C. B. Xu, Z. F. Ren, W. S. Yang, Z. B. Ma, D. X. Dai, H. J. Fan, T. K. Minton, X. M. Yang, *J. Chem. Soc.*, 134 (2012) 13366.

4. C. Arrouvel, S. C. Parker, M. S. Islam, *Chem. Mater.*, 21 (2009) 4778.
5. Z. Y. Sun, X. Huang, M. Muhler, W. Schuhmann, E. Ventosa, *Chem. Commun.*, 50 (2014) 5506.
6. D. J. Reidy, J. D. Holmes, C. Nagle, M. A. Morris, *J. Mater. Chem.*, 15 (2005) 3494.
7. T. Tachikawa, M. Fujitsuka, T. Majima, *J. Phys. Chem. C*, 111 (2007) 5259.
8. J. Y. Jiang, Z. Y. Huang, Y. Mi, Y. F. Li, A. Q. Yuan, *Proc. Chem.*, 22 (2010) 1058.
9. Y. Z. Wen, Y. Q. Xue, Z. X. Cui, Y. Wang, *J. Chem. Therm.*, 80 (2015) 112.
10. T. Kasuga, M. Hiramatsu, A. Hoson, T. Sekino, K. Niihara, *Adv. Mater.*, 11 (1999) 1307.
11. C. Kim, S. Kim, J. Choi, J. Lee, J. S. Kang, Y. E. Sung, J. Lee, W. C. J. Y., *Electrochim. Acta*, 141 (2014) 113.
12. R. Singh, R. Bapat, L. Qin, H. Feng, V. Polshettiwar, *ACS Catal.*, 6 (2016) 2770.
13. X. L. Yan, L. H. Jia, X. F. Guo, *Chinese J. Appl. Chem.*, 28 (2011) 278.
14. Q. J. Xiang, J. G. Yu, M. Jaroniec, *J. Am. Chem. Soc.*, 134 (2012) 6575.
15. K. Zhu, N. R. Miedaner, A. Miedaner, A. J. Frank, *Nano Lett.*, 7 (2007) 69.
16. S. Li, Y. M. Zhang, J. G. Huang, *J. Alloy Compd.*, 783 (2019) 793.
17. Y. H. Yao, J. Rong, J. F. Y. N. Zhang, X. W. X. H. Yu, Z. L. Zhan, *Ceram. Int.*, 45 (2019) 10845.
18. C. Y. Zhu, J. X. Liu, X. H. Yu, Y. N. Zhang, Y. J. Zhang, X. D. Jiang, S. Wang, Q. W. P. D., *J. Mater. Sci.*, 30 (2019) 5866.
19. Y. H. Yao, Z. T. Yuan, Y. N. Zhang, X. H. Yu, J. Rong, K. Meng, Z. L. Zhan, *Chinese J. Inor. Chem.*, 34 (2018) 662.
20. X. B. Chen, S. S. Mao, *Chem. Rev.*, 107 (2007) 2891.
21. Z. Wang, X. M. Xie, M. Jiang, C. Y. Yang, T. Q. Lin, H. Yin, *Energ. Environ. Sci.*, 6 (2013) 3007.
22. M. Wang, J. H. Zhu, Y. Q. Xue, Z. X. Cui, M. Z. Zhao, *J. Mater. Sci.*, 52(2017) 1039.
23. J. P. Du, R. H. Zhao, Y. Q. Xue, *J. Chem. Therm.*, 45(2012) 48.
24. L. D. Wang, Z. Y. Huang, G. C. Fan, Z. G. Zhou, X. C. Tan, *Sci. China Chem.*, 42 (2012) 47.
25. G. C. Fan, L. Sun, Z. Y. Huang, J. Y. Jiang, Y. F., *Mater. Lett.*, 65 (2011) 2783.
26. G. C. Fan, J. Chen, Y. J. Ma, Z. Y. Huang, *Micro. Nano Lett.*, 7 (2012) 795.
27. J. A. Dean. Lange's Handbook of Chemistry. 15th ed. New York: McGraw-Hill, 6 (1998) 1029.
28. J. Li, J. F. Huang, J. Y. Li, L. Y. Cao, H. Qi, Y. Y. Cheng, Q. Xin, H. Dang, *J. Alloy Compd.*, 727 (2017) 998.
29. M. A. Deyab, S. T. Keera, *Mater. Chem. Phys.*, 146 (2014) 406.
30. G. G. Zhang, C. J. Huang, L. M. Zhou, L. Ye, W. F. Li, H. T. Huang, *Nanoscale*, 3 (2011) 4174.
31. J. Li, J. F. Huang, J. Y. Li, L. Y. Cao, H. Qi, Q. Xin, Y. Y. Cheng, *J. Alloy Compd.*, 784 (2019) 165.
32. R. Meng, H. Hou, X. Liu, W. Hu, J. Duan, S. Liu, *Ceram. Int.*, 41 (2015) 9988.